

Recent advances in generation of terahertz vortex beams and their applications*

Honggeng Wang(王弘耿)^{1,2}, Qiyong Song(宋其迎)¹, Yi Cai(蔡懿)¹, Qinggang Lin(林庆钢)¹, Xiaowei Lu(陆小微)^{1,†}, Huangcheng Shangguan(上官煌城)¹, Yuexia Ai(艾月霞)¹, and Shixiang Xu(徐世祥)^{1,‡}

¹Shenzhen Key Laboratory of Micro-Nano Photonic Information Technology, College of Physics and Optoelectronic Engineering, Shenzhen University, Shenzhen 518060, China

²Key Laboratory of Optoelectronic Devices and Systems and Ministry of Education and Guangdong Province, College of Optoelectronic Engineering, Shenzhen University, Shenzhen 518060, China

(Received 13 May 2020; revised manuscript received 24 June 2020; accepted manuscript online 6 July 2020)

Last decade has witnessed a rapid development of the generation of terahertz (THz) vortex beams as well as their wide applications, mainly due to their unique combination characteristics of regular THz radiation and orbital angular momentum (OAM). Here we have reviewed the ways to generate THz vortex beams by two representative scenarios, i.e., THz wavefront modulation via specific devices, and direct excitation of the helicity of THz vortex beams. The former is similar to those wavefront engineering devices in the optical and infrared (IR) domain, but just with suitable THz materials, while the latter is newly-developed in THz regime and some of the physical mechanisms still have not been explained explicitly enough though, which would provide both challenges and opportunities for THz vortex beam generation. As for their applications, thanks to the recent development of THz optics and singular optics, THz vortex beams have potentials to open doors towards a myriad of practice applications in many fields. Besides, some representative potential applications are evaluated such as THz wireless communication, THz super-resolution imaging, manipulating chiral matters, accelerating electron bunches, and detecting astrophysical sources.

Keywords: terahertz vortex beams, wavefront modulation, orbital angular momentum, nonlinear optics

PACS: 74.25.Uv, 87.56.jk, 42.65.-k

DOI: [10.1088/1674-1056/aba2df](https://doi.org/10.1088/1674-1056/aba2df)

1. Introduction

In recent years, besides the development of efficient terahertz (THz) sources and detectors,^[1–3] the progress of THz optics is also mandatory to enable the specific control and manipulation of THz radiation through its amplitude, phase, polarization, and even orbital angular momentum (OAM), in which a forefront research area of THz radiation shaping situation corresponds to the generation of vortex THz radiation. THz vortex beams combine the merits of THz waves and OAM. In specific, THz waves have the highly coherent non-ionizing nature, wide unallocated frequency bands, distinctive wavelengths, and high penetration power, while OAM couples additional degree of freedom to matter. Accordingly, THz vortex beams have great potentials for many applications. For instance, THz beams with OAM can increase THz communication capacity due to an unlimited number of OAM eigenstates.^[4–6] THz vortex beams have the potential beyond the diffraction limit and to obtain super-resolution imaging with spatial resolution of micrometers.^[7–10] It can be applied to reveal terahertz nonlinearities in some materials like graphene.^[4] Since the elementary rotational and vibration excitations of many matters in nature are found in the THz frequency range,^[5,11–16] THz vortex beams can be employed in

manipulating these matters, such as DNA and protein,^[7,17–20] Bose–Einstein condensation currents in the solid state,^[21] and so on. Also, THz vortex beams are promising in acceleration and manipulation of electron bunches because they can offer shorter electron bunches and higher resolution with less infrastructures.^[22–26] Moreover, THz OAM beams could be used to detect and observe astrophysical sources, such as rotating black holes, masers, possibly the cosmic microwave background radiation, and so on.^[27–30] THz vortex beams are promising in even some uncharted territories, too.

Because of these numerous applications, researchers have been working on how to generate efficiently THz vortex beams for years. However, there have been very fewer reports about the vortex generation in THz domain. According to these reports, methods for THz vortex beam generation can be divided into two scenarios, as shown in Fig. 1.

In this paper, we focus on a comprehensive overview for the generation of THz vortex beams and some representative potential applications. This paper is organized as follows. Section 2 will review and discuss the methods for THz vortex beam generation. In Section 3, we will present some potential and promising applications of vortex THz radiation. Finally, a summary and outlook will be given in Section 4.

*Project supported partly by the National Natural Science Foundation of China (Grant Nos. 61775142 and 61705132) and Shenzhen Fundamental Research and Discipline Layout Project, China (Grant Nos. JCYJ20170412105812811, JCYJ20190808164007485, JCYJ20190808121817100, and JCYJ20190808115601653).

†Corresponding author. E-mail: xiaoweilu@szu.edu.cn

‡Corresponding author. E-mail: shxxu@szu.edu.cn

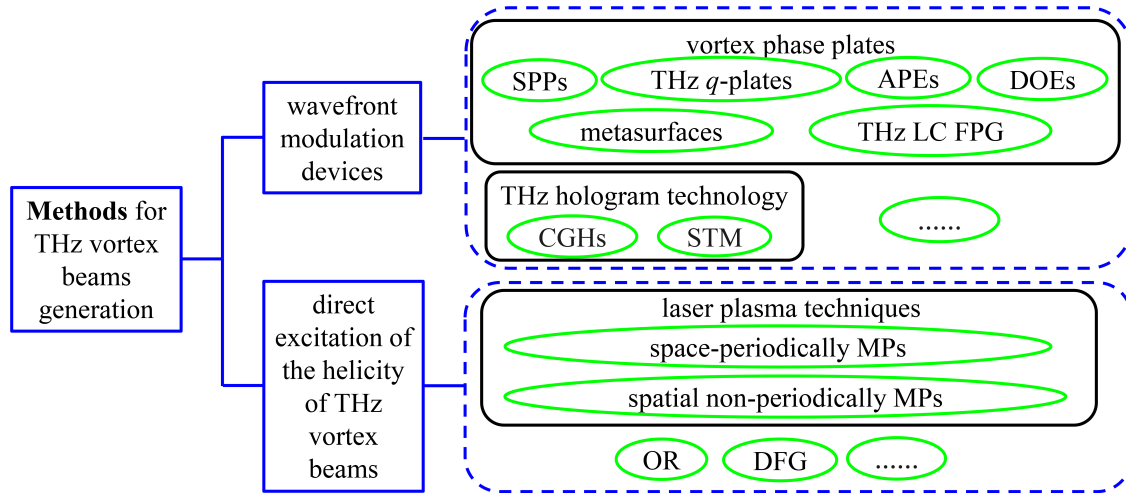


Fig. 1. Two scenarios of methods for THz vortex beam generation (SPPs: spiral phase plates, APEs: achromatic polarization elements, DOEs: diffractive optical elements, THz LC FPG: THz liquid crystal forked polarization grating, CGHs: computer-generated holograms, STM: spatial terahertz modulator, MPs: modulated plasmas, OR: optical rectification, DFG: difference-frequency generation).

2. Methods for THz vortex beam generation

The ways to produce THz vortex beams can be divided into two categories. One introduces OAM with some THz wavefront modulators, which is quite a straightforward strategy similar to the wavefront modulators in the optical and infrared (IR) domain and the other excites directly to generate THz vortex beams by using some vortex pump lasers and/or matters.

2.1. THz vortex beam generation by wavefront modulation devices

There are fewer THz wavefront modulation devices compared with those in the visible and IR domain due to a lack of materials for desired THz engineering.^[31] Fortunately, researchers have found that several superior materials are suitable for these manipulators. To be specific, most of them are some flexible polymeric materials with low permittivity, absorbance, and dispersion in THz regime,^[32,33] such as Tsurupica olefin polymer,^[8,10,34,35] polylactic acid (PLA) medium,^[36] polypropylene,^[37,38] polytetrafluoroethylene (Teflon),^[39–42] polyimide,^[43,44] polystyrene,^[45,46] nylon polyamide,^[47] acrylonitrile-butadiene-styrene,^[48] polyethylene,^[49] and so on. In addition, some special materials like graphene^[50–55] and plasma^[56] can also be applied to THz wavefront manipulators. Commonly, there are two ways to fabricate these devices by the materials mentioned above, one is only by mechanically polishing without any chemical processes,^[8,34–38] which is very easy; and the other is by a commercial three-dimensional (3D) printing technique,^[39,45,48,57] which is an efficient and low-cost method with good resolution.^[46,49,57] By and large, these THz wavefront modulation devices include vortex phase plates and THz hologram technology. More detailed descriptions are as follows.

2.1.1. Vortex phase plates

Several vortex phase plates have been already applied to produce THz vortex beams, such as spiral phase plates (SPPs), THz q -plates, achromatic polarization elements (APEs), diffractive optical elements (DOEs), metasurfaces, and THz liquid crystal (LC) forked polarization grating (FPG).

2.1.1.1. Spiral phase plates

Generally, an SPP is a refractive optical element that can impose azimuth dependent phase retardation with azimuthally varying thickness. Its step height can be expressed as

$$h = l\lambda / \Delta n. \quad (1)$$

Here l is the change in topological charge induced by the SPP, λ is the wavelength of the incident wave, and Δn is the difference of the refractive index between the SPP and surrounding medium. The total phase delay around the plate center is an integer multiple of 2π , i.e., $2\pi l$,^[38] as shown in Fig. 2. The transmission function of the SPP can be given by

$$u(r, \theta) = \text{circ}\left(\frac{r}{R}\right) \exp(i l \theta), \quad (2)$$

where r and θ are the radius and azimuthal coordinates in the polar coordinate, respectively, and i is the imaginary unit. R is the effective aperture (EA) of the SPP, while $\text{circ}(\cdot)$ is the circular function. According to Eq. (2), SPPs can be considered as phase-only elements. Up to date, the reported materials for THz SPPs include Tsurupica olefin polymer,^[8,34] polylactic acid (PLA) medium,^[36] Teflon,^[39–41] polypropylene and polypropylene-like materials.^[37,38,48] Apart from the polypropylene and polypropylene-like materials that are suitable in the 3D printing technique according to the adaptive-additive algorithm^[58] or pattern search optimization algorithm,^[37] the others are used to fabricate SPPs by mechanically polishing. Additionally, by using an SPP together with a Teflon axicon,^[59,60] thereby to possess thickness gradients in both radial and azimuthal directions, an incident Gaussian

beam has been converted into a high-order Bessel beam with spiral phase structure,^[59] which can work in the center frequency of 0.3 THz^[59] or 0.5 THz.^[60]

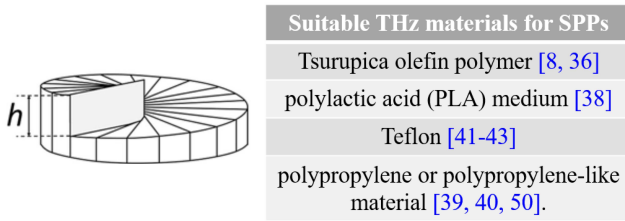


Fig. 2. 3D model of an SPP with proper THz materials. Reproduced with permission from Ref. [34].

Generally speaking, SPPs are very simple and economical, and can be applied to the pulses with any polarization states. Furthermore, one SPP can be used to generate OAM beams with two conjugated topological charges just by getting the SPP reversed. Additionally, SPPs are easy to produce high-order, free-space Laguerre–Gaussian (LG) beams. However, the size of SPPs with high-order topological charges needs a higher spatial resolution. Moreover, SPPs are not pure mode converters. The purity of LG beams produced by them is limited by the co-production of undesirable higher-order modes with radial index p and topological charge l , i.e., LG_{pl} .^[61] Also, they are typically designed for a certain frequency and a certain topological charge. Hence, they would exhibit topological-charge dispersion for broadband sources. An additional limitation of the stepped SPPs is diffraction from the step edges depending on the manufacturing technique and the step edge width. Now wide applications of the SPPs make it urgent demand to develop new materials suitable for THz regime and to improve the fabricated methods which would avoid the problem of narrow bandwidth, strong diffraction effect, discontinuous profile, and so on.

2.1.1.2. THz q -plates

A q -plate is a pure geometrical phase optical element that enables the realization of vector beams and vortex beams with a simple and compact optical design. It is a thin optical birefringent waveplate with the space-dependent orientation of the ordinary and extraordinary axes in the transverse plane.^[46,62,63] Its fast axes have certain topological structures, rather than a homogeneous structure like a half-wave plate. The number q , which denotes the changing rate of the optical axis with respect to the azimuthal angle, depicts the specific geometry. Usually, the number q is an integer or a semi-integer. This device is mainly used in optics to generate some structured beams, which are inhomogeneous but contain particular phases or polarization singularities. In a q -plate, the optical axis orientation α with respect to the x axis follows $\alpha(r, \theta) = q\theta + \alpha_0$, where r and θ are the polar radius and the azimuthal angle, respectively, and α_0 is the initial angle

when $\theta = 0$. There are some examples of q -plates shown in Fig. 3.^[62] It implies the presence of a defect in the material localized at the plane origin, i.e., $r = 0$. And the Jones matrix of a q -plate is given by^[45]

$$H = \begin{pmatrix} \cos 2\alpha & \sin 2\alpha \\ \sin 2\alpha & -\cos 2\alpha \end{pmatrix}. \quad (3)$$

In order to generate a vortex beam, an original circularly polarized pulse with desired handedness is needed, which can be obtained by employing an adequately oriented THz quarter-wave plate. A circularly polarized laser beam after passing through the q -plate is converted to one with the opposite circular polarization, and more importantly, to a helical wavefront.^[63] If the output from the q -plate then passes through another properly oriented quarter-wave plate and a linear polarizer, the complex amplitude of the electric field can be calculated by

$$\begin{aligned} E_{\text{out}} &= \begin{pmatrix} \cos 2\alpha & \sin 2\alpha \\ \sin 2\alpha & -\cos 2\alpha \end{pmatrix} \begin{pmatrix} 1 & 0 \\ 0 & -1 \end{pmatrix} \begin{pmatrix} 1 \\ \pm i \end{pmatrix} \begin{pmatrix} 1 & 0 \\ 0 & 0 \end{pmatrix} \\ &= \exp(\pm 2i\alpha) \begin{pmatrix} 1 \\ 0 \end{pmatrix}, \end{aligned} \quad (4)$$

where “+” and “-” correspond to left and right circular polarizations, respectively. As a result, an OAM variation of $\pm 2\alpha\hbar$ (\hbar is the reduced Planck constant) is imposed, which means a linearly polarized vortex beam with its topological charge of 2α would be produced.^[64] In other words, q -plates can couple spin angular momentum (SAM) to OAM, without changing the total angular momentum.

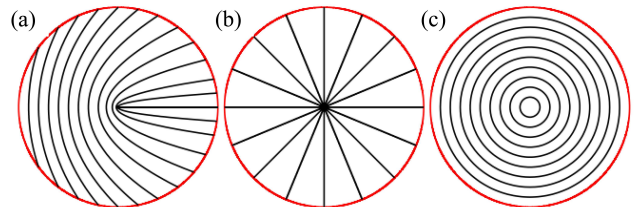


Fig. 3. Three examples of q -plates. The tangent to the lines shown indicates the local direction of the optical axis. (a) $q = 1/2$ and $\alpha_0 = 0$, which can generate helical modes with $l = \pm 1$; (b) $q = 1$ and $\alpha_0 = 0$, (c) $q = 1$ and $\alpha_0 = \pi/2$, which both can generate helical modes with $l = \pm 2$. Reproduced with permission from Ref. [62].

Some materials can be used to fabricate THz q -plates like nematic LC, polystyrene, quartz crystal, even plasma. In specific, nematic LC has proven to be a very promising candidate for THz q -plates in a frequency range from 0.5 THz to 2.5 THz due to the pronounced optical birefringence, controllable director (i.e., local optical axis) distribution, and external field responsiveness.^[43,44,65] By exploiting electro-optic effect in LCs, real-time control of the retardation of LC-based q -plates is available through an externally applied voltage.^[66] An alternative 3D printing material for THz q -plates is polystyrene, which is a highly transparent material at the frequency of 0.15 THz, or at the wavelength of 2 mm.^[47,48] Quartz crystal can also be suitable for THz q -plates. It has a relatively large transmission coefficient for a wide spectral range from

0.1 THz to 2.5 THz. This THz q -plate is made of space-variant birefringent slabs endowed with an azimuthally varying in-plane optical axis orientation by mechanically polishing, i.e., segmented half-wave plate.^[64] Interestingly, the plasma q -plate can work in a broad frequency range spanning from THz to the optical domain^[56] with an external axial-symmetric magnetic field controlling the optical fast axes. The laser mode conversion relies on the anisotropy of the dispersion relation in the magnetic field. As a result, a direct transformation of the optical angular momentum from the spin form to the orbital form takes place. We note that this is a rather counterintuitive process, in which the input polarization of light controls the shape of the output wavefront.^[62]

The THz q -plate is single and compact, and also has high stability in the long term and requires almost no maintenance. The device works in transmission geometry and therefore is free of many alignment problems. The device can be used to create a superposition of SAM/OAM states with no need of interferometric setups. The conversion efficiency (the ratio of OAM-converted THz radiation power over total transmitted light power) is relatively high. Moreover, several q -plates can be predicted to arrange in cascade, which is able to address a large range of OAM values.^[67] However, q -plates require specialized polarization (i.e., circularly-polarized), low-power input laser modes, and complex surface geometries, which limits their usability. Their efficiency depends intensely on the wavelength of the incident waves. Mostly, the reported THz q -plates are designed based on 3D printing technology. The structures with discontinuous features are difficult to print with reasonable quality.^[45] THz q -plates exhibit relatively low damage threshold and severe transmission loss. In addition, until now, the reported q -plates are restricted to azimuthally variant optical axes. If we can overcome this limit, the capability of wavefront manipulation will be drastically enhanced; therefore, more complex beam shaping will be achievable.

2.1.1.3. Achromatic polarization elements

Theoretically, a THz radially polarized beam can be converted into a THz vortex pulse by an APE, which consists of an achromatic quarter-wave plate and a wire-grid polarizer with specific fast axes orientations.^[68,69] The achromatic quarter-wave plate can be made by high-resistance silicon, which has a high transmission coefficient in the wide range from 1 THz to 2.5 THz. After passing through a quarter-wave plate with its fast axis parallel to the x axis, a THz radially polarized beam with L -th azimuthal order ($L \geq 0$) becomes

$$\begin{aligned} E_{QR} &= \begin{bmatrix} 1 & 0 \\ 0 & i \end{bmatrix} E_0(r; \omega) \begin{bmatrix} \cos L\theta \\ \sin L\theta \end{bmatrix} \\ &= E_0(r; \omega) \begin{bmatrix} \cos L\theta \\ i \sin L\theta \end{bmatrix}, \end{aligned} \quad (5)$$

where $E(r; \omega)$ is the electric field in the frequency domain, which does not depend on the azimuthal angle θ . Further-

more, if E_{QR} goes through a polarizer whose transmission axis is 45° from the x axis, the output THz field can be described as

$$\begin{aligned} E(r; \theta; \omega) &= \frac{\sqrt{2}}{2} (\cos L\theta + i \sin L\theta) E_0(r; \omega) \\ &= \frac{\sqrt{2}}{2} E_0(r; \omega) \exp(iL\theta). \end{aligned} \quad (6)$$

Therefore, the phase of the THz wave φ equals to $L\theta$, which indicates that the THz wave is a vortex beam with the topological charge of $l = L$. The above conversion process can be depicted in Fig. 4.

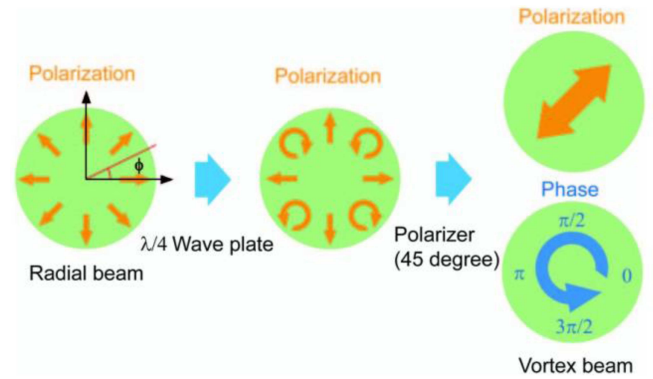


Fig. 4. Schematic of the conversion process by APEs. Reproduced with permission from Ref. [68].

In APEs, incoming THz radially polarized beams are required. However, the direct conversion of the IR vector beam into the THz vector beam in ZnTe crystal is only reported when the beam collinearly propagates along the $\langle 111 \rangle$ axis of the ZnTe crystal possessing threefold rotational symmetry.^[70] Moreover, this threefold crystal is not commonly used in the THz community since the THz generation efficiency is much lower than that by the $\langle 110 \rangle$ ZnTe crystal.

2.1.1.4. Diffractive optical elements

There are some types of staircaselike DOEs reported to generate THz vortex beams, such as binary phase spiral Fresnel plates (BPSFPs),^[71] binary phase spiral axicons (BPSAs),^[72] the combination of an optimal phase element (OPE) and a Fourier transform (FT) lens (OPE+FT).^[49,57] The first two elements (BPSFPs and BPSAs) can be applied to generating non-diffractive THz Bessel vortex beams. The last one (OPE+FT) is used to produce THz circular Airy vortex beams^[49] or THz perfect optical vortex beams.^[57] Note that a perfect vortex can be described by a series expanded in terms of Bessel functions of the same order and different scales theoretically.^[73] Its OPE (for example, spatial light modulators (SLMs),^[58] diffractive optical phase plates,^[49] and so on) can form an optimal phase mask to impose the phase modulation, and its FT lens can perform the FT. Figure 5 shows the phase profiles of two BPSAs. Here we take BPSFPs as an example.

BPSFPs can be designed by silicon binary phase plates with the spiral configuration of zones, whose prototype is an

amplitude Fresnel zone plate reported in Ref. [74]. In simple terms, when a spherical wave interferes with a vortex beam, the interference intensity pattern can be described as

$$I \propto 1 + \cos \left[l\theta - k \left(1 + \frac{1}{2}r^2 \right) \right], \quad (7)$$

where r and θ are the radius and azimuthal coordinates, respectively, while k and l are the wave number and the topological charge, respectively. The boundary between a bright fringe and a dark fringe occurs when the above cosine term is zero. When the beams are collinear, it means

$$l\theta - k \left(1 + \frac{1}{2}r^2 \right) = \left(n + \frac{1}{2} \right) \pi, \quad (8)$$

where $n = 0, \pm 1, \pm 2, \dots$. According to the above, BPSFPs can be produced by filling in the region where the modulation term is negative. Equation (8) can be generalized for modes with a topological charge of l . Note that $l=0$ corresponds to the standard Fresnel zone plate.

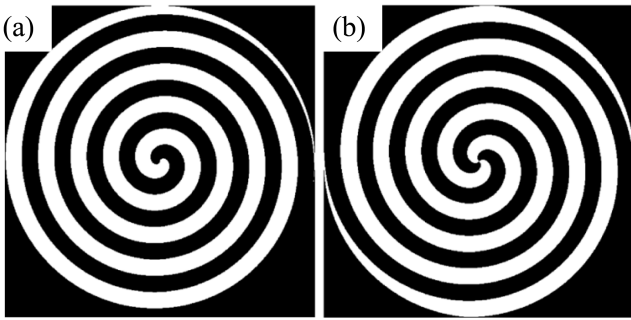


Fig. 5. Phase profiles of two BPSAs. (a) $l = \pm 1$; (b) $l = \pm 2$. Reproduced with permission from Ref. [57].

Generally, DOEs provide a flexible method to generate OAM beams and allow for *in situ* adjustment of the diffraction pattern. The sign of the topological charge determines the direction of the spiral rotation. In addition, DOEs have high efficiency and resolution and are not sensitive to polarization of the incident laser light. Most DOEs are designed only to generate Bessel vortex beams. Certainly, it is also desirable to design DOEs to produce more complex THz vortex patterns.[75–78]

2.1.1.5. Metasurfaces

Metasurfaces, some ultrathin metamaterials consisting of planar subwavelength units, have been used to achieve phase modulations covering a full range of 360° .^[50] They can be divided into two categories based on the phase modulation mechanism: resonance-based metasurfaces^[4,79–82] and geometric-phase metasurfaces.^[68,83,84] The former can be engineered as SPPs, while the latter is designed to behave like q -plates, which transfer SAM to OAM based on Pancharatnam–Berry (PB) phase principle.

There are several typical metasurfaces reported for THz vortex beam generation based on the aforementioned two categories. The resonance-based metasurfaces in THz domain are reported, such as V-shaped slit antennas structure,^[79,80] anisotropic chiral metasurface,^[81] resonant-tunneling-diode oscillators by integrated radial line slot antenna,^[82] and multifunctional graphene metasurfaces.^[4] While the geometric-phase metasurfaces for THz vortex beam generation include circular sub-wavelength slits,^[83] reflective metasurface structure,^[84] double-ring distributed slit array,^[85] etc. Here we take the V-shaped slit antennas structure and circular sub-wavelength slits as examples. Figure 6 shows their schematic structures.

The complementary V-shaped slit antennas structure was fabricated on a thin metal film (100 nm Au).^[79] It is on a double-side polished high resistivity silicon substrate of 500 μm thickness with conventional photolithography and metallization process. Each antenna unit is composed of two equivalent rectangular slits which are connected at one end in a square region with a length of 200 μm . The slit width is fixed at 5 μm . The slit length, the angle between two slits, and the angle between the bisector line of the V-shaped antenna and the y axis can be adjusted to achieve the phase modulation of the scattered field. It should be noted that the selection of the complementary structure is to make sure the high diffraction efficiency of the THz vortex beams. The designed central wavelength of the metasurface was reported at 400 μm corresponding to 0.75 THz.^[79]

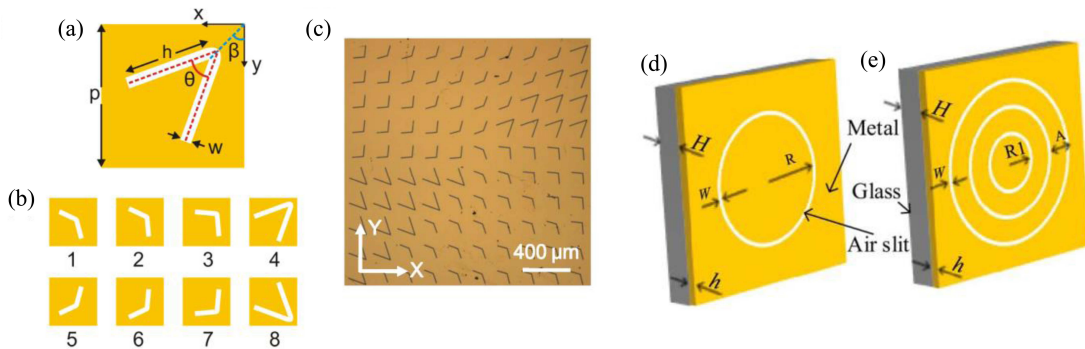


Fig. 6. Schematic structure of two representative metasurfaces. (a)–(c) V-shaped slit antennas structure; (d)–(e) circular sub-wavelength slits. Reproduced with permission from Refs. [79,83].

By contrast, the circular sub-wavelength slit structure^[83] has a good response over a broad bandwidth from 0.3 THz to 3 THz. There is a circular sub-wavelength air slit in a 200-nm silver film, which can be regarded as a localized linear polarizer with radial direction,^[86] so such a device can act as an axially symmetric polarizer (ASP) whose transmission axis is radially distributed.^[87,88] The Jones matrix of the ASP is given by

$$P = \begin{pmatrix} \cos^2 \theta & \cos \theta \sin \theta \\ \cos \theta \sin \theta & \sin^2 \theta \end{pmatrix}, \quad (9)$$

where θ is the azimuth angle in the beam cross section.

When a circularly polarized THz wave incidents normally upon the thin film, the output complex amplitude in the near-field zone can be expressed as

$$\begin{aligned} E_{\text{out}}(r, \theta; \omega) &= \begin{pmatrix} \cos^2 \theta & \cos \theta \sin \theta \\ \cos \theta \sin \theta & \sin^2 \theta \end{pmatrix} \begin{pmatrix} 1 \\ \pm i \end{pmatrix} E_0(r; \omega) \\ &= E_0(r; \omega) \exp(\pm i\theta) \begin{pmatrix} \cos \theta \\ \sin \theta \end{pmatrix}, \end{aligned} \quad (10)$$

where $E(r; \omega)$ is the amplitude in the frequency domain, independent of θ . Equation (10) indicates that this device can transfer the SAM to OAM ($\pm \hbar$) of the incident THz beams. The output electric field is radially polarized, i.e., it is a radially polarized THz vortex beam.

In contrast to the traditional bulk optical elements, metasurfaces provide a perspective on shaping flexibly the electromagnetic field by manipulating the phase, amplitude as well as polarization at will via a compact and easy-of-fabrication system.^[51] Another advantage of metasurfaces is tunability, which can be achieved by manipulating and controlling the interaction between the metasurfaces and the incident waves to modify the transmission, reflection, and absorption of the incident waves according to the desired functionalities. Most metasurfaces for THz vortex beam generation are structured by metallic cells. They possess high losses due to the skin effect in the THz region, and few reach a 360° phase adjustment, which affects the accuracy. Emphasis should be placed on some suitable, flexible, and low-loss materials in the THz frequency.

2.1.1.6. THz liquid crystal forked polarization grating

When a gradient blazed phase is introduced into a common spiral phase, the integrated phase profile in the xy plane shall be^[89,90]

$$\phi(x, y) = l\theta - 2\pi x/\Lambda, \quad (11)$$

where l is the topological charge, $\theta(x, y) = \arctan(y/x)$ exhibits the local azimuthal angle in the xy plane, and Λ is the

pitch. The first and second terms on the right-hand side describe a common spiral phase and the introduced blazed phase, respectively. The phase distributions of a spiral phase, a blazed phase, and their integration with $l = 1$ and $\Lambda \approx 1.2$ mm are shown in Figs. 7(a)–7(c), respectively. The ideal 3D LC waveplate has a sawtooth-shaped profile consisting of blazed grating and substrate, as shown in Fig. 7(d). The integrated phase is fork-like with a space-variant change. Such fork phase profiles can be obtained by PB phase, which results from an LC waveplate with space-variant axis orientation (α) as following:

$$\alpha(x, y) = \phi(x, y)/2 = l\theta/2 - \pi x/\Lambda. \quad (12)$$

The LC waveplates with such gradient-rotation directors are denoted as LC FPG. The diffraction property can be theoretically analyzed through the Jones matrix calculation.^[91] The Jones matrix of the FPG is given by^[90]

$$\begin{aligned} J(x, y) &= R(-\alpha) \begin{pmatrix} \exp(-i\Gamma/2) & 0 \\ 0 & \exp(i\Gamma/2) \end{pmatrix} R(\alpha) \\ &= \cos \zeta \begin{pmatrix} 1 & 1 \\ 1 & 1 \end{pmatrix} - i \sin \zeta \begin{pmatrix} \cos 2\alpha & \sin 2\alpha \\ \sin 2\alpha & -\cos 2\alpha \end{pmatrix}. \end{aligned} \quad (13)$$

Here $\Gamma = 2\pi\Delta n d/\lambda$ is the phase retardation, $\zeta = \Gamma/2$ is the normalized retardation, λ is the free-space wavelength, d is the cell gap, and Δn is the LC birefringence. When a circularly polarized beam passes through such an LC FPG, the emerging wave can be expressed as

$$\begin{aligned} D(x, y) &= J(x, y) E(x, y) \\ &= \cos \zeta \begin{pmatrix} 1 \\ \pm i \end{pmatrix} - i \sin \zeta \exp[\pm i l \theta(x, y) \mp i 2\pi x/\Lambda] \begin{pmatrix} 1 \\ \mp i \end{pmatrix}. \end{aligned} \quad (14)$$

The far-field electric field of the n -th order diffraction is^[89]

$$\begin{aligned} D_n(x, y) &= \frac{1}{\Lambda} \int_0^\Lambda D(x, y) \exp(-i 2\pi x/\Lambda) dx \\ &= \cos \zeta \delta_n \begin{pmatrix} 1 \\ \pm i \end{pmatrix} - i \sin \zeta \delta_{n\pm 1} \exp[\pm i l \theta(x, y)] \begin{pmatrix} 1 \\ \mp i \end{pmatrix}, \end{aligned} \quad (15)$$

where δ_n and $\delta_{n\pm 1}$ are Dirac delta functions. The FPG has three diffraction orders: ± 1 st orders are always circularly polarized and orthogonal to each other with conjugated topological charges, while the 0th order is a Gaussian beam with the same polarization as the input one. The intensity distributions among these three orders depend on the phase retardation and the incident polarization.

A THz LC FPG can be used to generate and separate simultaneously pure THz vortex beams with conjugated circular polarization. However, it is bulky, and its fabricating process is very difficult and complicated.^[92]

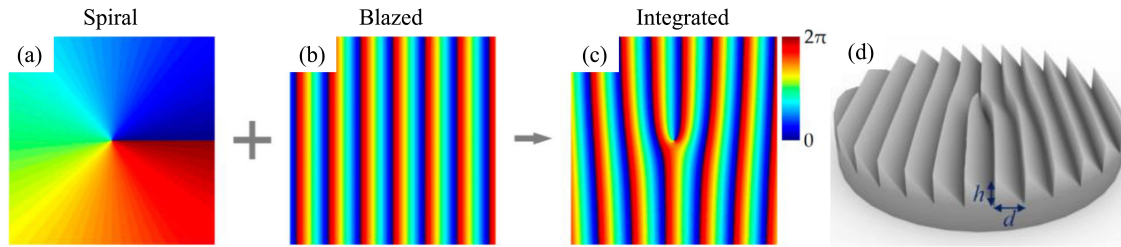


Fig. 7. Phase presentation and idea 3D schematic structure of THz LC FPG. (a) A common spiral phase distribution; (b) introduced gradient blazed phase distribution; (c) integrated phase distribution; (d) ideal 3D LC FPG. Reproduced with permission from Refs. [89,90].

2.1.2. THz hologram technology

Hologram technology can also be utilized to generate THz vortex beams. Some reported works include computer-generated holograms (CGHs) and spatial terahertz modulator (STM). The former operates at the sub-THz frequency range, such as 0.119 THz,^[93] 0.31 THz,^[94–96] 0.65 THz,^[94] and so on, while the latter works in a range of 1–1.6 THz.^[97]

2.1.2.1. THz computer-generated holograms

CGHs are locally periodic diffraction gratings that modify both the reflected and transmitted electromagnetic fields.^[94,98] The hologram structure can be numerically designed and then printed or etched on the hologram substrate material. The holograms are often locally binary, i.e., the grating structure consists of a single groove with width w and depth h . The grating period d is the local spatial period of the transmittance; it satisfies the grating equation $\sin \theta_{\text{out}} = \sin \theta_{\text{in}} + m\lambda/d$, where θ_{in} and θ_{out} are the incident and diffraction angles, respectively, and m is the diffraction order in question.^[90] There are two types of holograms to generate Bessel vortex beams in the sub-THz regime, i.e., amplitude-type holograms and phase-type holograms,^[94] whose local grating structures are shown in Fig. 8.

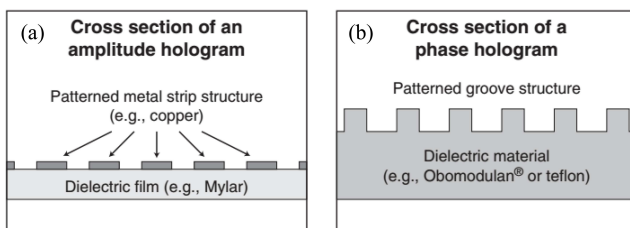


Fig. 8. Local grating structures. (a) Amplitude holograms; (b) phase holograms. Reproduced with permission from Ref. [94].

In an amplitude-type hologram, its diffraction grating consists of copper stripes (17 μm) on a dielectric Mylar film (75 μm thick, relative permittivity $\epsilon_r = 3.3$). The designed pattern can be fabricated using photolithography and chemical wet etching.^[98] The skin depth of sub-THz wave within the copper is far less than 1 μm . Therefore, the metallic grating effectively reflects all the field which includes incident beams on the copper stripe and transmitted beams through the slots between the stripes. Consequently, the transmitted field is effec-

tively modulated with a binary function and then diffracted according to the wavelength-scale structure caused by the hologram grating. The phases and amplitudes are modulated by the locations of the slots and the variations of the slot widths, respectively. Typically, the available signals are those from the first diffraction orders generated by the holograms. Such an amplitude-type hologram can also indirectly modulate the phases of the 1st order diffraction field, as the phases can be coded in the positions of the copper strips.^[99]

While in the phase-type holograms, the hologram structure features locally change the effective thickness seen by the electromagnetic waves which can be realized by varying either the refractive index or the depth of the surface profiles. The hologram elements consist of milled grooves on a dielectric substrate (obomodular[®], $\epsilon_r \approx 2.2$). The sub-THz field passing through the grooves acquires a phase difference with respect to that between the grooves, leading to phase modulation of the transmitted field, instead of amplitude modulation. There are, however, always some losses due to both the reflection of the electric field on the interface of a dielectric material and the attenuation within a lossy dielectric. The groove profile of a phase hologram may be binary (all grooves have rectangular cross sections), multilevel (stepped profile), or continuous. Rigorous electromagnetic modeling is required to optimize the grating structure.^[94,100,101]

Since binary holograms are cheap and easy to fabricate, and typically suitable for sub-THz regime, they are useful in real-world applications of OAM. In reality, these holograms are with wavelength-scale diffractive structures, and the modulations of their amplitudes are never purely binary, so further optimization is usually necessary by rigorous modeling methods.^[100]

2.1.2.2. Spatial terahertz modulator

An STM requires an array of small building blocks that can independently control the transmission or reflection of a THz beam at different positions. Hence, the transparency at different positions of the semiconductor wafer can be independently modulated. Specifically, the control beam modulated by a conventional SLM illuminates the surface of a 500 μm thick semiconductor silicon wafer to produce the corresponding pattern of photo-generated carriers, whose prototype is

shown in Fig. 9. Its intrinsic broadband response results in the relatively broad bandwidth (1–1.6 THz) of the generated THz vortex beams.^[97] The transmission for the THz beam is governed by the spatial distribution of photo-generated carriers, which form an amplitude hologram. Compared with the electrically controlled THz spatial modulator,^[102] the all-optically controlled STM has higher resolution (better than 140 μm) and better modulation depth.

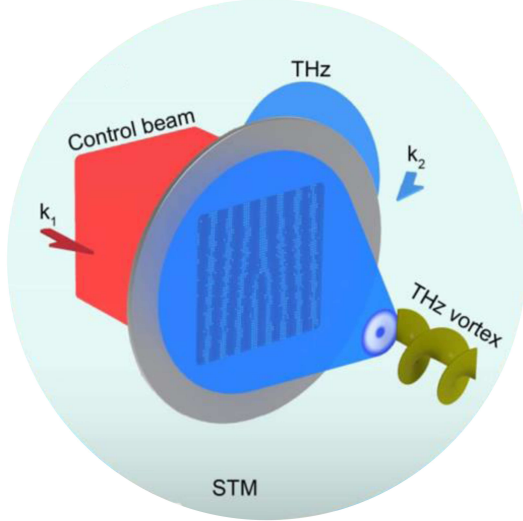


Fig. 9. Prototype of STM. Reproduced with permission from Ref. [97].

The STM allows the all-optical or electrical control of the spatial transmission or reflection of an input THz wave; therefore, it can encode the information in a wavefront, and produce broadband THz vortex beams.^[97] The modulation of the STM is limited by the optical SLM, which is expensive. Unfortunately, SLM has usually low laser damage threshold, thereby fails to bear the high intensity of laser pulses.

The above devices discussed in Subsection 2.1 are basically designed to manipulate the regular THz beams with a specific topological charge and a given frequency, or with a relatively narrow bandwidth. These elements are lack of tunability, switchability, and versatility inherently, which are key requirements to handle the wavefront of THz pulses. Furthermore, their bandwidths are still not enough to develop tunable THz vortex beams.

2.2. Directly exciting the helicity of the THz vortex beams

So far, there are also some reports on directly exciting the OAM of the THz vortex beams. These reported methods include optical rectification (OR), difference-frequency generation (DFG), and laser plasma techniques.

2.2.1. Optical rectification

THz beams can be generated by OR of an IR laser pulse in a $\langle 110 \rangle$ ZnTe crystal. Both pulses are assumed to propagate

along the \hat{x} axis in the Cartesian frame $(\hat{x}, \hat{y}, \hat{z})$ of the laboratory, which coincides with the $\langle 110 \rangle$ axis of the crystal (see Fig. 10).^[103]

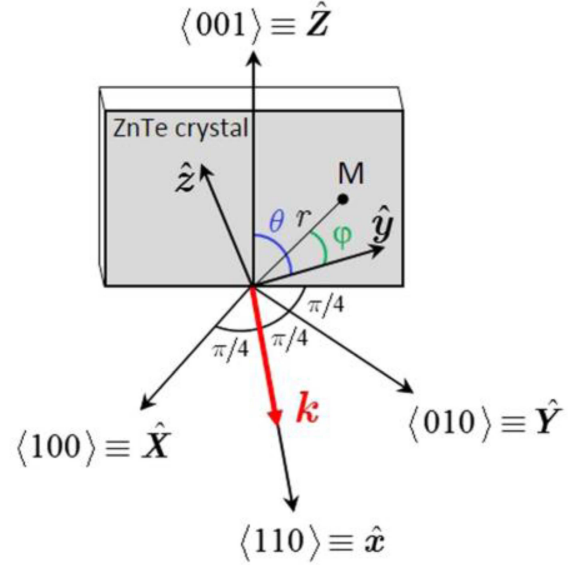


Fig. 10. Geometry of $\langle 110 \rangle$ ZnTe crystal. Reproduced with permission from Ref. [103], ©The Optical Society.

Considering an incident IR vector pulse with azimuthal order l , the electric field can be written as^[104]

$$\mathbf{E} = E_0(r) [\cos(l\theta) \hat{y} + \sin(l\theta) \hat{z}], \quad (16)$$

where $r = \sqrt{y^2 + z^2}$ and θ are the radius and azimuth of the polar coordinate system in the plane of the crystal, respectively, while $E(r)$ is the amplitude of a Gaussian laser beam. According to the relation $\mathbf{E}^{\text{THz}} \propto \partial^2 \mathbf{P}^{(2)} / \partial t^2$, we can get

$$\begin{pmatrix} E_x^{\text{THz}} \\ E_y^{\text{THz}} \\ E_z^{\text{THz}} \end{pmatrix} = E_0'(r) \begin{pmatrix} 0 \\ 3 \cos(3\varphi - 2l\theta) - \cos(\varphi - 2l\theta) - 2 \cos(\varphi) \\ 3 \cos(3\varphi - 2l\theta) + \sin(\varphi - 2l\theta) - 2 \sin(\varphi) \end{pmatrix}, \quad (17)$$

where $E_0'(r)$ is the amplitude of the THz Gaussian beam with a $1/e$ beam waist w_{THz} . Since the incoming IR laser beam is azimuthally polarized, there is no preferential orientation for IR electric field. Without loss of generality, one can select $\varphi = 0$, so the components of the THz electric field in the frame of the laboratory become^[103]

$$\begin{pmatrix} E_x^{\text{THz}} \\ E_y^{\text{THz}} \\ E_z^{\text{THz}} \end{pmatrix} = -\frac{1}{2} E_0'(r) \begin{pmatrix} 0 \\ \sin^2(l\theta) \\ \sin(2l\theta) \end{pmatrix} \\ = -\frac{1}{4} E_0'(r) \begin{pmatrix} 0 \\ 1 - (e^{2il\theta} + e^{-2il\theta}) / 2 \\ (e^{2il\theta} - e^{-2il\theta}) / i \end{pmatrix}. \quad (18)$$

Equation (18) reveals that the output of the THz electric field is a combination of three terms with the topological charges of 0, $2l$, and $-2l$, respectively. One can remove either the topological $+2l$ or $-2l$ via appropriate polarization projection by using a quarter waveplate and a polarizer. After passing through a quarter waveplate with its fast axis parallel to the

y axis followed by a polarizer whose transmission axis is oriented at an angle α from the y axis, the THz electric field is polarized in the α direction and expressed as

$$\begin{aligned} E_{\alpha}^{\text{THz}} &= E_y^{\text{THz}} \cos \alpha + i E_z^{\text{THz}} \sin \alpha \\ &= -\frac{1}{4} E_0'(r) \left[\cos \alpha + \left(\sin \alpha - \frac{\cos \alpha}{2} \right) e^{2i\theta} \right. \\ &\quad \left. - \left(\sin \alpha + \frac{\cos \alpha}{2} \right) e^{-2i\theta} \right], \end{aligned} \quad (19)$$

when $\tan(\pm\alpha) = \pm 1/2$ (i.e., $\alpha = 0.46$ rad), the vortex component $2l$ or $-2l$ will vanish. So

$$E_{\pm\alpha}^{\text{THz}} = -\frac{1}{2\sqrt{2}} E_0'(r) \left(1 - e^{\mp 2i\theta} \right). \quad (20)$$

Accordingly, the generated THz electric field by OR along the polarizer axis is not a pure vortex pulse. It is a superposition of a Gaussian field (topological charge $l = 0$) and a vortex field with the topological charge of $+2l$ or $-2l$.

In general, OR is well suited for intense THz vortex generation — one can simply increase the surface area of the OR crystal with more input laser energy and efficient phase-matching condition. The bandwidth depends on the frequency response of the OR crystal. However, until now, using OR still fails to generate pure THz vortex pulses.

2.2.2. Difference-frequency generation

There are two schemes reported to generate THz vortex beams by DFG. The first one bases on type-II DFG between

two collinear near-infrared (NIR, 800 nm) chirped pulses with orthogonal polarizations, conjugated topological charges, and a relative time delay.^[105] A $\langle 110 \rangle$ ZnTe crystal was used in DFG process at 800 nm. The 800 nm pulses were generated collinearly with a passive and transmissive device, which consists of a polarizer, a q -plate, a quarter waveplate, a wedge-plate pair, and a focal lens, shown in Fig. 11(a). The chirp was introduced to suppress the THz radiation from OR, which also results in low DFG efficiency. When the fast axis of the quarter waveplate is $+45^\circ$ or -45° from the horizontal direction, and the topological charge of the q -plate is $q = 1/2$, the output electric field behind the device shown in Fig. 11(a) can be described as

$$\begin{aligned} E_{\text{out}} &= \begin{pmatrix} 1 & \mp i \\ \mp i & 1 \end{pmatrix} \begin{pmatrix} \cos \theta & \sin \theta \\ \sin \theta & -\cos \theta \end{pmatrix} \begin{pmatrix} 1 & 0 \\ 0 & 0 \end{pmatrix} \begin{pmatrix} E_x \\ E_y \end{pmatrix} \\ &= e^{-i\theta} \begin{pmatrix} E_x \\ 0 \end{pmatrix} - i e^{i\theta} \begin{pmatrix} 0 \\ E_x \end{pmatrix} \quad \text{or} \quad e^{i\theta} \begin{pmatrix} E_x \\ 0 \end{pmatrix} + i e^{-i\theta} \begin{pmatrix} 0 \\ E_x \end{pmatrix}. \end{aligned} \quad (21)$$

Equation (21) implies that the pulses can be regarded as the combination of a pair of pulses with orthogonal polarizations and conjugated topological charges, i.e., $l_1 = 1, l_2 = -1$ or $l_1 = -1, l_2 = 1$. It implies that the polarization of the two 800 nm vortex pulses can be easily exchanged by changing the fast axis of the quarter waveplate.

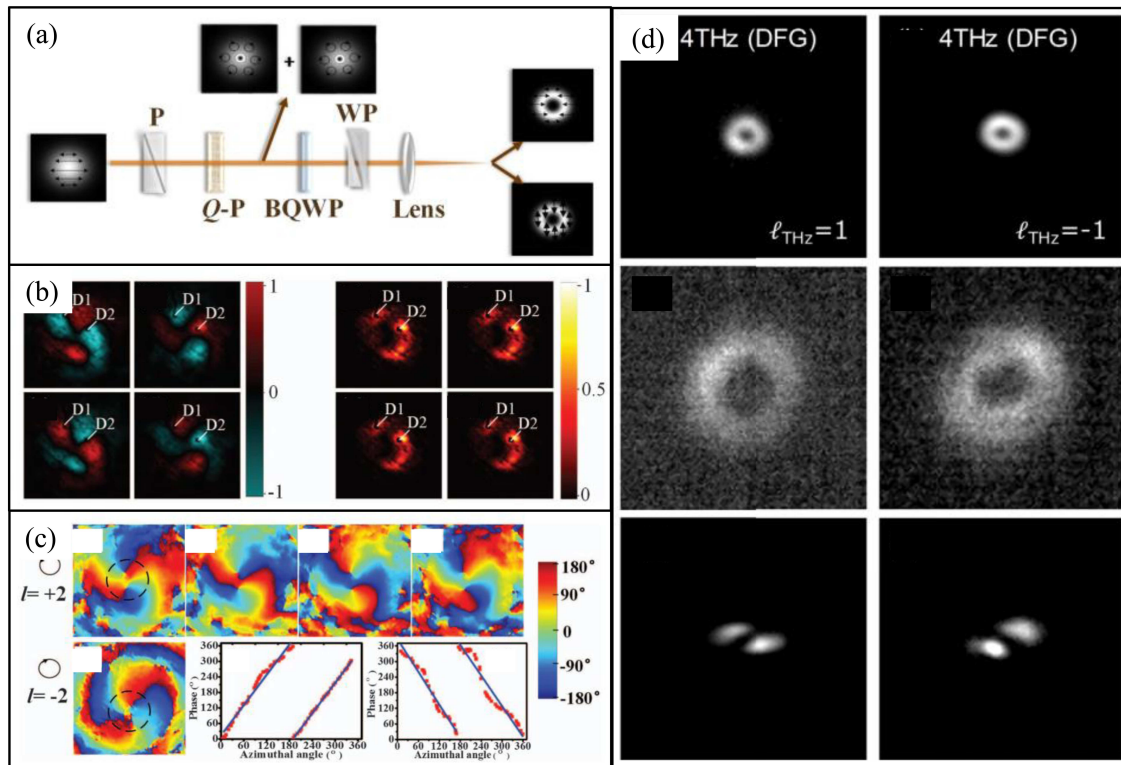


Fig. 11. Some experimental devices for a pair of 800 nm vortex beams and some experimental results for THz vortex beam generation. (a) Passive and transmissive device of generating collinear vortex pulse pair of 800 nm with conjugated topological charges and orthogonal polarizations. P, polarizer; Q-P, q -plate; BQWP, broadband quarter-wave plate; WP, wedge-plate pair; (b) experimental spatial amplitude and intensity distributions of the THz vortex pulses at different time delays in Ref. [105]; (c) corresponding phase distributions of the THz vortex pulses at different time delays in Ref. [105]. (d) Experimental far- and near-fields of 4 THz vortex beams with the topological charge of ± 1 in Ref. [10]. Reproduced with permission from Refs. [10,105], ©The Optical Society.

The complex amplitude of generated THz beams A_{THz} by type-II DFG can be described by^[105,106]

$$\frac{dA_{\text{THz}}(r, \omega_{\text{THz}}, z)}{dz} \propto -i\kappa [E_1(r, \omega_1, z)][E_2(r, \omega_2, z)]^* \\ = -i\kappa E_{10}(r, \omega_1, z) E_{20}^*(r, \omega_2, z) \exp[i(l_1 - l_2)\theta], \quad (22)$$

with

$$E_1(r, \omega_1, z) = E_{10}(r, \omega_1, z) \exp(il_1\theta), \quad (23)$$

$$E_2(r, \omega_2, z) = E_{20}(r, \omega_2, z) \exp(il_2\theta), \quad (24)$$

where κ is the coupling constant. The frequencies of the interactive three waves satisfy the relation $\omega_{\text{THz}} = \omega_1 - \omega_2$. Equation (22) implies that the topological charge of the THz pulse is the difference between the topological charges of the two conjugated NIR pulses, i.e., $l_{\text{THz}} = l_1 - l_2$. The central frequency of the generated THz vortex is about 2 THz with multi-cycles in Ref. [105]. The spatial amplitude, intensity, and phase distributions of the THz vortex pulses at different time delays are shown in Figs. 11(b) and 11(c).

In the second setup, a vortex beam (1.56 μm) and a Gaussian beam (1.5–1.64 μm) generated by two optical parametric amplifiers (OPA1 and OPA2) are focused and spatially overlapped on a 4'-dimethylamino-N-methyl-4-stilbazolium tosylate (DAST) crystal to generate the high-quality THz vortex mode within the frequency range of 2–6 THz via soft-aperture DFG.^[10] The output beam from OPA1 is transferred to a vortex via an SPP, which provides only an azimuthal phase shift of $2l\pi$ to a fundamental Gaussian pulse. The generated vortex beam typically includes undesirable higher-order radial LG modes.^[61] When the vortex beams and the Gaussian beams are superimposed spatially, one can find that the individual radial modes with multiple rings in the vortex output are spatially separated in the far-field. According to the DFG principle, it is noteworthy that the focused Gaussian mode plays a role as a soft-aperture to remove undesired high-order radial LG modes.^[10] According to the OAM conservation law, the topological charge of THz should satisfy the following relationship:

$$l_{\text{THz}} = (l_{\text{OPA1}} - l_{\text{OPA2}}) \frac{\lambda_{\text{OPA2}} - \lambda_{\text{OPA1}}}{|\lambda_{\text{OPA2}} - \lambda_{\text{OPA1}}|}, \quad (25)$$

where l_{THz} , l_{OPA1} , and l_{OPA2} are the topological charges of the THz, OPA1, and OPA2 outputs, respectively. λ_{OPA1} and λ_{OPA2} are the wavelengths of the OPA1 and OPA2 outputs, respectively. Figure 11(d) shows the experimental far- and near-fields of 4 THz vortex beams with the topological charges of ± 1 .

One of DFG advantages is tunability. The spectra of the generated THz vortex beams are limited by the frequency responses of the used nonlinear DFG crystals.

2.2.3. Laser plasma techniques

So far, there are two types of laser plasma techniques reported to generate THz vortex beams, namely,

space-periodically modulated plasmas (MPs) and spatial non-periodically MPs.

2.2.3.1. Space-periodically modulated plasmas

Recently, a few schemes for generating THz vortex beams have been proposed based on space-periodically MPs, which include rippled plasmas (RPs) and vortex plasmas (VPs).

The plasma density of a RP can be defined as^[107]

$$n_{\text{RP}} = n_0 + n_q = n_0 + n_{q0} \exp(iqz), \quad (26)$$

where n_{q0} is the amplitude of the ripple and q is the wave number of the density ripple, while n_0 is the background electron density. This periodic plasma density (ripple) can be considered as a slow structure and can be created by various methods. In the RP, THz vortex can be produced by propagating two coaxial LG laser beams (frequencies ω_1 , ω_2 ; wave numbers k_1 , k_2 ; topological charges l_1 , l_2). The LG laser beams have nonuniform spatial profiles in the radial direction. This nonuniform profile creates a refractive index gradient in the radial direction, which is responsible for the nonuniform ponderomotive force in the plasma channel. When an intense laser beam propagates in plasma, due to the transverse intensity gradient, the ponderomotive force pushes the electrons out of high intensity regions. As a result, the plasma density varies and causes a change in the dielectric function, which starts behaving like a lens, thereby results in stronger self-focusing of the laser in turn. On the other hand, due to diffraction, the defocusing of the laser beam takes place. From the focusing–defocusing, a density-modulated filament occurs. Due to the intensity variation in the transverse direction, the nonlinear plasma current emerges at the beating frequency. The current has superluminal Fourier components, which can emit a THz vortex pulse. The selection rule is $l_{\text{T}} = \tilde{l} \pm 1$, where $\tilde{l} = l_1 - l_2$.^[107] Figure 12(a) shows the simulation results of THz vortex beam generation via RP. If the RP is submerged in a static electric field, a new selection rule will be available, i.e., $|l_{\text{T}} - \tilde{l}| \leq 1$, where l_{T} is an integer.^[107] By selecting a suitable plasma distribution, only one of the OAMs can be produced. Note that the THz electric field can increase tremendously by enhancing the ripple density amplitude. It seems that this increase is more pronounced near the resonant excitation of the THz wave, the wave number of the RPs is given by

$$q_{\text{S}} = \frac{\tilde{\omega}}{c} \left[\left(1 - \frac{\omega_{\text{p}}^2}{\tilde{\omega}^2} \right)^{1/2} - 1 \right]. \quad (27)$$

Here $\omega_{\text{p}} = (4\pi e^2 n_0 / m_e)^{1/2}$ is the plasma frequency, while e , m_e , n_0 and c are the electron charge, electron mass, the background electron density, and speed of light in vacuum, respectively.

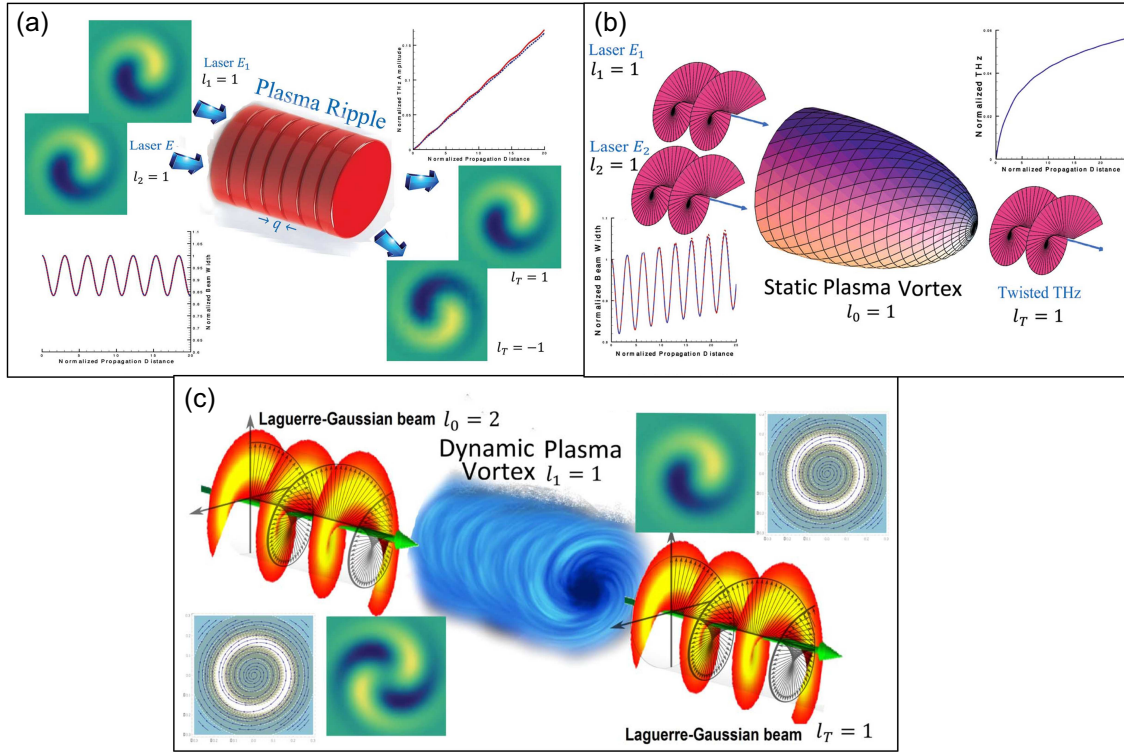


Fig. 12. Simulation results of the generation of THz vortex beams via a type of (a) RPs; (b) SVPs; and (c) DVPs. Reproduced with permission from Ref. [107]. ©The Optical Society.

While in VP, the OAM exchange occurs between it and the emitted THz radiation.^[107] Actually, the VP is a kind of special plasma by adding a helical structure into a RP. Namely, its electric density distribution is a function of space and/or time with a helical structure. Generally, two kinds of VPs have been outlined as the static vortex plasmas (SVPs) and the dynamic vortex plasmas (DVPs). The electron density distribution of the SVPs, described in space coordinates (r, θ, z) , depends on the distance with respect to the vortex axis of symmetry and is allowed to vary slowly along z , while the electron density of the DVPs is defined as a function of space and time coordinate $(r, \theta, t; z)$.^[107] The SVPs and DVPs can be respectively defined as

$$n_{\text{SVP}} = n_0 + n_S = n_0 + n_{S0} \exp(iq_S z + i l_S \theta), \quad (28)$$

$$\begin{aligned} n_{\text{DVP}} &= n_0 + n_D \\ &= n_0 + n_{D0} \exp(-iq_D z + i\omega_D t - i l_D \theta), \end{aligned} \quad (29)$$

where t , r , and θ are the temporal coordinate, the radius and azimuthal coordinates in the polar coordinate. n_0 is the background electron density. l_S , q_S , and n_{S0} are the topological charge, wave number, and amplitude of SVPs, while q_D , l_D , and n_{D0} are the wave number, topological charge, and amplitude of DVPs, respectively. ω_D is the frequency of the Langmuir/plasma wave. For a SVP with $l_S \neq 0$ or a DVP with $l_D \neq 0$, the OAM of the electron and ion plasma waves is nonzero.^[107] SVPs are considered as collisional plasmas.

When the duration of the incident laser is equal to or greater than the electrons energy relaxation time, the collisional nonlinearity becomes dominant while the ponderomotive force nonlinearity can be ignored. By propagation of two LG laser pulses with the same OAM or even the two Gaussian pulses without OAM (their frequencies are ω_1 and ω_2 , their wave numbers are k_1 and k_2 , their topological charges are l_1 and l_2 , respectively; for Gaussian pulses, their topological charges are zero, i.e., $l_1 = l_2 = 0$), the redistribution of electron density takes place in the transverse plane. The nonlinear current density is created at the beating frequency $\tilde{\omega} = \omega_1 - \omega_2$ with $\tilde{k} = k_1 - k_2$ and $\tilde{l} = l_1 - l_2$, which is responsible for THz vortex beam generation. The THz vortex beam generation can be described by OAM conservation law which is satisfied in the phase-matching condition by the RP^[107] with $k_T = \tilde{k} + q_S$. The topological charge of the THz radiation is $l_T = \tilde{l} + l_S$. To match the OAM of the electron plasma wave with the charge number of the SPVs, a part of the lasers' OAM is transferred to the electron plasma wave and the remaining part causes the torsion of the emitted THz wavefront.^[107] For two LG lasers with the same topological charges, even two Gaussian pulses (i.e., $\tilde{l} = l_1 - l_2 = 0$), the topological charge of the THz vortex beams is $l_T = l_S$, which indicates that the helical structure of the SPV excites the OAM of the THz radiation. By contrast, in the DVPs, instead of the collisional nonlinearity, the ponderomotive force nonlinearity is dominant. There are two

types of pump laser pulses which can interact with a DVP. One is LG laser (l, ω), and the other is Langmuir wave with a THz frequency (l_L, ω_L). The beating ($\omega_T = \omega_0 - \omega_D$ or $\omega_T = \omega_L + \omega_D$) causes nonlinear current density generation. Correspondingly, the THz vortex beams at the beat frequency are generated based on the transformation of the OAM between plasma and laser. The OAM conversion law is also satisfied in the phase-matching condition of the RPs. Likewise, the OAM of the incident laser is divided into two parts: one part for OAM of the DVP, and the other part for the THz photons. In the quantum picture, a virtual quanta has been considered to explain the exchange of the OAM between the laser and medium. Specifically, the helical structure of the DVP provokes the plasma electron velocity with vortex number $-l_D$, opposite to that of the virtual quanta OAM l_D . Besides, if the input laser is polarized circularly, the THz vortex beams will generate with a circular polarization. As a result, a new OAM selection rule for THz vortex generation via DVPs is $l_T = l_0 - l_D$ or $l_T = l_L + l_D$, which correspond to the two different beating processes $\omega_T = \omega_0 - \omega_D$ or $\omega_T = \omega_L + \omega_D$. Figures 12(b) and 12(c) illustrate the OAM selection rules for generating THz vortex beams via SVPs and DVPs, respectively.

The space-periodically MPs can produce THz vortex beams with a specific topological charge by choosing suitable plasma density distribution. In order to generate such space-periodically MPs, many methods are explored, but the implementation of such plasmas is not straightforward, and it suffers from low efficiency, too.

2.2.3.2. Spatial non-periodically modulated plasmas

Laser-induced gas plasmas by a two-color field (a fundamental wave and its second harmonics) or a few-cycle ultrashort pulse can be considered as spatial non-periodically MPs, which are exclusive to achieve a high intensity and broad bandwidth regular THz field beyond the damage threshold of bulk materials.^[108–111] Recent researchers found that these two fields with OAM, i.e., two-color vortex field (Gaussian 800 nm + vortex 400 nm) or a few-cycle vortex field (vortex 800 nm), can induce millimeter-scale gas-plasma to generate ultra-broadband intensity modulated THz vortex waves, which are also called THz angular accelerating beams.^[112–114] Some experimental and simulation results for the generation of the intensity modulated THz vortex beams in Refs. [113,114] are shown in Fig. 13. Note that angular accelerating beams are tailored to have a nonlinear phase variation with azimuthal angle, which indicates angular acceleration.^[113] Its bandwidth can even reach 50 THz, and its topological charge can be inherited from the driving laser, namely, the topological charge of the second harmonic vortex pulse or that of the few-cycle vortex pulse. Moreover, the phase nonlinearity and the intensity distribution intensely depend on the frequencies of ultra-broadband THz radiation. The degree of nonlinearity determines the magnitude of the angular acceleration and deceleration.^[113] One can infer that the spatial non-periodically MPs are a promising way to develop THz vortex sources with broad bandwidth and high power.

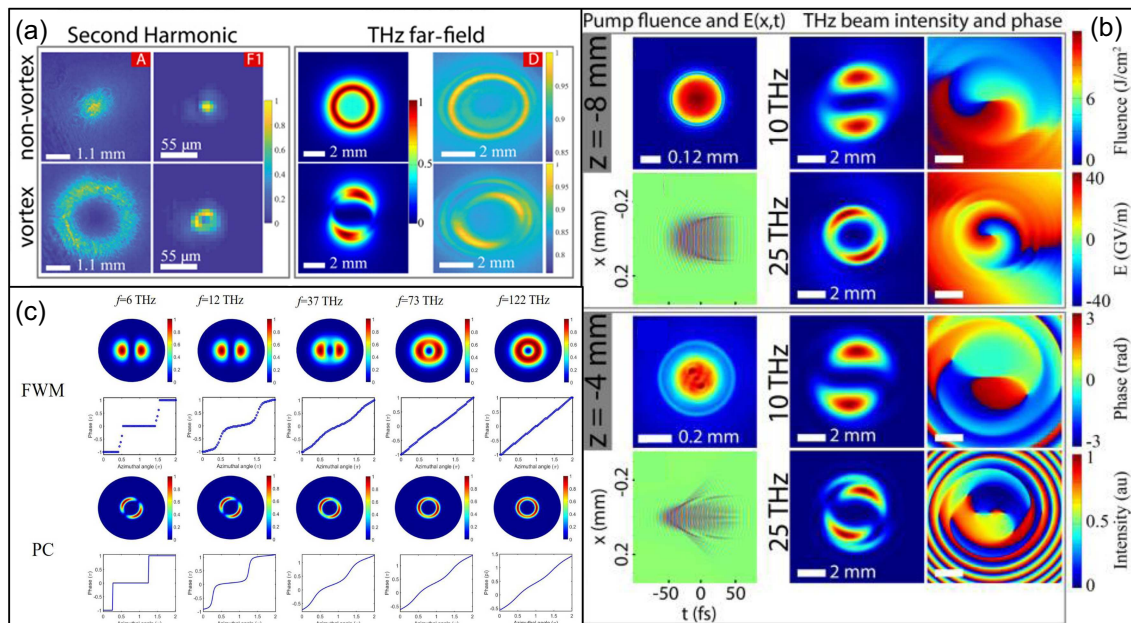


Fig. 13. Some experimental and simulation results of intensity modulated THz vortex beam generation via two-color or few-cycle vortex pump laser. (a) Experimental fluencies of Gaussian and vortex second harmonics, corresponding simulating and experimentally far-field THz fluencies in two-color vortex pump field case; (b) simulating fluency and electric field of two-color pump and corresponding far-field intensity and phase of two frequency components of THz pulses in two-color vortex pump field case in Ref. [114]; (c) simulating intensity and phase distributions of different frequency components of THz pulses in few-cycle vortex pump field case in Ref. [113]. Reproduced with permission from Refs. [113,114], ©The Optical Society.

On the one hand, typically, most inert gases such as N_2 , He, Ar, and so on can be used as the media to generate spatial non-periodically MPs, and thus radiate THz pulses.^[108–111] Recently, researchers found that some liquids like water, ethanol, and acetone could be promising to produce plasma filaments, thereby generating broadband intense THz radiation.^[115–117] So far, it is more complicated to understand the THz radiation from liquid-plasmas than that from gas-plasmas. On the other hand, the spatial non-periodically MPs can be easily produced and their spatial structures and lengths can be modulated by the different pump laser modes focusing conditions and so on. Up to now, various excitation wavelengths, media, and focusing conditions have been explored in order to maximize THz wave radiation from laser-induced plasmas, while few attempts have been made with artificially modulated exotic spatial structures of pump laser field.^[118,119] It has been found that the exotic spatial structures could affect the density distribution and spatial shape of the laser-induced plasmas, thereby change the intensity and even phase distributions of the generated THz radiation. One can predict that the motion of free electrons in plasmas induced by pump vortex laser pulses would be more complicated. Liquid-plasmas excited by pump vortex field could be expected to generate stronger vortex THz radiations than gas-plasmas, which is one of the hotspots in nonlinear THz optics and THz photonics.^[118] However, how the OAM and singularity of the pump vortex laser pulses affect the motion of free electrons in plasmas is unclear. To date, the underlying physical mechanisms of these gas-plasmas induced by vortex pump laser pulses have not been explained clearly enough, too, which would provide both challenges and opportunities for THz vortex beam generation. Such plasma-based THz emitters can avoid the limitation to material ionization threshold. These THz vortex sources with the wide tunability and broad bandwidth are strongly desired for applications.

3. Potential applications of THz vortex beams

Thanks to the advent and continuous development of THz optics and singular optics, many applications of THz vortex beams have been made possible, such as optical tweezers, optical wrenches, cell rotators and stretchers in biomedical engineering and medical fields. Going beyond conventional THz photonics, manipulating the wavefront of THz radiation opens new opportunities that underpin application areas in THz wireless communication, THz super-resolution imaging, manipulation of chiral matters, acceleration of electron bunches, detection of astrophysical sources, and so on.

3.1. THz wireless communication

With the increasing demand for higher bandwidth and bigger capacity of the wireless communication system, the

extension of the operating frequency of the communication system to the THz wave regime is inevitable.^[11,18,120–122] Furthermore, apart from the well-known physical parameters of electromagnetic waves like amplitude, phase, time, frequency, and polarization, there is always interest in exploiting new degrees of freedom like OAM to get ever-higher data capacity in wireless communications.^[48] A beam carrying OAM can provide an infinite range of possibly achievable states because OAM modes form a complete and orthogonal basis. Communication utilizing such orthogonal modes could increase the capacity of communication by the number of additional spatially orthogonal modes.^[123] Consequently, one can infer that THz vortex pulses with huge under-exploited bandwidth and an unlimited number of OAM eigenstates could provide higher channel capacity and carrier frequency, bigger data transmission rate (> 10 Gbit/s), better confidentiality, better anti-interference ability, high-definition videos at live broadcast sites for high-speed THz wireless communication systems.^[4,6,114–130] Recent reports show that several basic functionalities, e.g. multiplexing/demultiplexing, have already been realized for THz vortex beams communications.^[48,124,131,132] Scientists also predict that outdoor wireless communication will soon be available at a rate of 40 Gbit/s without any difficulties, and may increase to 100 Gbit/s — fast enough to download a typical movie in seconds. The performance of indoor use, which is technically easier than outdoor use, would strongly depend on the application and its market.^[11,120,126,127]

3.2. THz super-resolution imaging

THz imaging technologies show great potentials when it comes to nondestructive testing and biomedical sensing. However, the resolutions of conventional THz imaging systems are constrained by the diffraction limit.^[133–136] Generally, there are two main approaches to improve the spatial resolution of THz imaging. One is to enhance the imaging systems, while the other is to develop novel super-resolution methods,^[137] including operation with THz vortex beams.^[138] The spatial resolution of the regular THz imaging is usually limited to the sub-millimeter scale due to the diffraction limited resolution.^[11,139,140] THz vortex pulses have the potential to break through the limitation of diffraction and to obtain an ultrahigh spatial resolution at a spatial resolution of micrometers by applying it to materials with nonlinearities such as saturable absorption, up-conversion excitation, and stimulated emission in THz region,^[9,10,141] which would allow the observation of local defects in crystalline materials such as graphene^[142] and various semiconductors.^[143–146] Such THz super-resolution imaging will open the door towards next-generation molecular sciences, biomedicine, security inspection, nondestructive detection, and so on.

3.3. Manipulation of chiral matters

As is known to all, chirality is used for describing the symmetry properties of an object. A chiral object, which cannot be superposed with its mirror by rotations or translations, is one of quite ubiquitous and exciting phenomena in the micro and macro world, such as protein, DNA, hands, shells, and etc. There are two types of chirality, i.e., one is left-handed, and the other is right-handed. Whereas objects in nature seem to prefer one chirality, for example, DNA is right-handed; almost all the natural amino acids are left-handed. Interestingly, vortex beams can be chiral by carrying OAM. On the other hand, the elementary excitations of many matters in nature have been found in the THz frequency range, such as the vibration frequencies of biomacromolecule (e.g., DNA, protein, and so on),^[8,9,18–21] phonon frequencies of Bose–Einstein condensation in the solid state,^[21,147] plasma frequencies, and so forth. Accordingly, the THz vortex beams have attracted more and more interest and can be employed in chemistry and biology. For instance, they can be applied to fabricate 3D chiral microstructures,^[21,148–150] which can be used to detect the chirality of material with the OAM. Moreover, vortical dichroism can be induced on the chiral microstructures by THz vortex beams instead of circularly polarized beams.

3.4. Acceleration of electron bunches

Acceleration and manipulation of electron bunches underline most electron and x-ray devices used for ultrafast imaging and spectroscopy. THz vortex beams are also promising in acceleration and manipulation of electron bunches. New THz-vortex-driven concepts could offer orders-of-magnitude improvements in field strengths, field gradients, laser synchronization, and compactness relative to conventional radio-frequency devices, enabling shorter electron bunches and higher resolution with less infrastructure while maintaining high charge capacities, repetition rates, and stability.^[22–26,151]

3.5. Detection of astrophysical sources

Recently, the properties of beams carrying OAM have attracted attention for practical astronomical applications.^[152] Concurrently, the radiation frequencies of many astrophysical sources are in THz frequency range, such as rotating black holes, masers, possibly the cosmic microwave background radiation and so on.^[27–30] In observational astronomy, OAM of vortex light including potential THz vortex beams can improve the resolution of diffraction-limited optical instruments by overcoming the Rayleigh separability criterion for the superposed LG beams,^[153,154] which predicts that it may offer the observation and detection of stellar separation. Bright scattered starlight limits high-contrast imaging to large angular offsets.^[155] One could improve the capability of direct observation of weak extrasolar planets hid-

den in the glare of a bright coherent source with high contrast imaging by “peering into the darkness” of an optical vortex coronagraph in THz domain.^[28,155–157] Due to the gravitational Faraday effect^[158] and the gravitational Berry phase effect,^[159,160] light propagating near rotating black holes experiences behavior analogous to light propagating in an inhomogeneous, anisotropic medium in which SAM-to-OAM conversion occurs.^[45] To detect rotating black holes, it will be sufficient to use the available THz telescopes, provided that they are equipped with proper OAM diagnostic instrumentation.^[152,161] Therefore, THz vortex beams show great promise in these applications^[162,163] for broader exploration.

4. Summary and outlook

This paper provides an overview of the generation of vortex THz radiation and some of its potential applications. Generally speaking, there are two scenarios of methods to generate THz beams with OAM: one is via wavefront modulation devices to engineer the wavefront of regular THz waves; and the other is through exciting the helicity of the THz vortex from the incident vortex beams and/or special media. The limitation of the former is the lack of suitable and desired materials for THz waves, and the devices in the former also suffer from relatively narrow bandwidth for the THz vortex beams. While the latter can work with relatively high pump laser power with broad bandwidth despite of relatively low conversion efficiency. It is newly-developed where some of the physical mechanisms still have not been explored explicitly, so there will be full of both challenges and opportunities therein. As for applications, one can foresee a historic breakthrough for science and technology through THz vortex pulses research. It is also noteworthy that the research of THz vortex waves is built on many areas of science. Activities and efforts geared towards the implementation of applications of THz vortex waves are unbounded. THz vortex beams are promising in the fields of observational astronomy, material science, biomedicine, nondestructive super-resolution molecular spectroscopy, and even some uncharted territories. Among these applications, sometimes, the THz vortex radiation sources with high power and broad bandwidth are required, besides sensitive sensors and detectors, and functional THz devices and materials.

In recent years, several breakthroughs related to the sources of THz vortex beam generation have essentially bridged the OAM-based THz technological gap and fashioned their sovereignty over the current and future cutting-edge technologies. Promisingly, future directions and emerging areas of interests will be identified with translating these methods into practical devices.

References

- [1] Zhang X C, Shkurinov A and Zhang Y 2017 *Nat. Photon.* **11** 16
- [2] Pererira M F and Shulika O V 2014 *Terahertz and Mid Infrared Radiation: Detection of Explosives and CBRN (Using Terahertz)* (Netherlands: Springer)
- [3] Lewis R A 2014 *J. Phys. D: Appl. Phys.* **47** 374001
- [4] Zhang C, Deng L, Zhu J, Hong W, Wang L, Yang W and Li S 2018 *Materials* **11** 1054
- [5] Kampfrath T, Tanaka K and Nelson K A 2013 *Nat. Photon.* **7** 680
- [6] Koenig S, Lopez-Diaz D, Antes J, Boes F, Henneberger R, Leuther A, Tessmann A, Schmogrow R, Hillerkuss D, Palmer R, Zwick T, Koos C, Freude W, Ambacher O, Leuthold J and Kallfass I 2013 *Nat. Photon.* **7** 977
- [7] Pickwell E and Wallace V P 2006 *J. Phys. D: Appl. Phys.* **39** R301
- [8] Miyamoto K, Kang B J, Kim W T, Sasaki Y, Niinomi H, Suizu K, Rotermund F and Omatsu T 2016 *Sci. Rep.* **6** 38880
- [9] Watanabe T, Iketaki Y, Omatsu T, Yamamoto K, Sakai M and Fujii M 2003 *Opt. Express* **11** 3271
- [10] Miyamoto K, Sano K, Miyakawa T, Niinomi H, Toyoda K, Vallés A and Omatsu T 2019 *Opt. Express* **27** 31840
- [11] Tonouchi M 2007 *Nat. Photon.* **1** 97
- [12] Mittleman D M 2018 *Opt. Express* **26** 9417
- [13] Kawase K, Ogawa Y, Watanabe Y and Inoue H 2003 *Opt. Express* **11** 2549
- [14] Hangyo M 2015 *Jpn. J. Appl. Phys.* **54** 120101
- [15] Ju L, Geng B, Horng J, Girit C, Martin M, Hao Z, Bechtel H A, Liang X, Zettl A, Shen Y R and Wang F 2011 *Nat. Nanotechnol.* **6** 630
- [16] Dhillon S S, Vitiello M S, Linfield E H, et al. 2017 *J. Phys. D: Appl. Phys.* **50** 043001
- [17] Humphreys K, Loughran J, Gradziel M, Lanigan W, Ward T, Murphy J and O'Sullivan C 2004 *Proceedings of the 26th Annual International Conference of the IEEE EMBS*, September 1–5, 2004, San Francisco, USA, p. 1302
- [18] Taylor Z D, Singh R S, Bennett D B, Tewari P, Kealey C P, Bajwa N, Culjat M O, Stojadinovic A, Lee H, Hubschman J P, Brown E R and Grundfest W S 2011 *IEEE T. THz Sci. Techn.* **1** 201
- [19] Walther M, Fischer B M, Ortner A, Bitzer A, Thoman A and Helm H 2010 *Anal. Bioanal. Chem.* **397** 1009
- [20] Suen J Y, Tewari P, Taylor Z D, Grundfest W S, Lee H, Brown E R, Culjat M O and Singh R S 2009 *Stud. Health Technol. Inform.* **142** 364
- [21] Omatsu T, Chujo K, Miyamoto K, Okida M, Nakamura K, Aoki N and Morita R 2010 *Opt. Express* **18** 17967
- [22] Zhang D, Fallahi A, Hemmer M, Wu X, Fakhari M, Hua Y, Cankaya H, Calendron A L, Zapata L E, Matlis N H and Kärtner F X 2018 *Nat. Photon.* **12** 336
- [23] Vieira J and Mendonça J T 2014 *Phys. Rev. Lett.* **112** 215001
- [24] Hebling J, Fülöp J A, Mechler M I, Pálfalvi L, Töke C and Almási G 2011 arXiv:1109.6852
- [25] Silenko A J, Zhang P and Zou L 2017 *Phys. Rev. Lett.* **119** 243903
- [26] Zheng H, Mirsaidov U M, Wang L W and Matsudaira P 2012 *Nano Lett.* **12** 5644
- [27] Tamburini F, Thidé B, Molina-Terriza G and Anzolin G 2011 *Nat. Phys.* **7** 195
- [28] Harwit M 2003 *Astrophys. J.* **597** 1266
- [29] Sanchez D J, Oesch D W and Reynolds O R 2013 *Astron. Astrophys.* **556** A130
- [30] Thidé B, Then H, Sjöholm J, Palmer K, Bergman J, Carozzi T D, Istomin Y N, Ibragimov N H and Khamitova R 2007 *Phys. Rev. Lett.* **99** 087701
- [31] Chan W L, Chen H T, Taylor A J, Brener I, Cich M J and Mittleman D M 2009 *Appl. Phys. Lett.* **94** 213511
- [32] Podzorov A and Gallot G 2008 *Appl. Opt.* **47** 3254
- [33] Walia S, Shah C M, Gutruf P, Nili H, Chowdhury D R, Withayachumnankul W, Bhaskaran M and Sriram S 2015 *Appl. Phys. Rev.* **2** 011303
- [34] Miyamoto K, Suizu K, Akiba T and Omatsu T 2014 *Appl. Phys. Lett.* **104** 261104
- [35] Kang B J, Miyamoto K, Kim W T, Ahn K J, Omatsu T and Rotermund F 2018 *Conference on Lasers and Electro-Optics Pacific Rim (CLEO-PR)* July 29–August 3, 2018, W4C.6.
- [36] Wang X, Shi J, Sun W, Feng S, Han P, Ye J and Zhang Y 2016 *Opt. Express* **24** 7178
- [37] Schemmel P, Pisano G and Maffei B 2014 *Opt. Express* **22** 14712
- [38] Schemmel P, Maccalli S, Pisano G, Maffei B and Ng M W R 2014 *Opt. Letters* **39** 626
- [39] Petrov N V, Kulya M S, Tsympkin A N, Bespalov V G and Gorodetsky A A 2016 *IEEE T. THz Sci. Techn.* **6** 464
- [40] Semenova V A, Kulya M S, Petrov N V, Grachev Y V, Tsympkin A N, Putilin S E and Bespalov V G 2016 *41st International Conference on Infrared, Millimeter and Terahertz Waves (IRMMW-THz)*, September 25–30, 2016
- [41] Semenova V, Kulya M and Bespalov V 2016 *J. Phys.: Conf. Ser.* **735** 012064
- [42] Wakayama T, Higashiguchi T, Oikawa H, Sakaue K, Washio M, Yone-mura M, Yoshizawa T, Tyo J S and Otani Y 2015 *Sci. Rep.* **5** 9416
- [43] Wang L, Lin X W, Liang X, Wu J B, Hu W, Zheng Z G, Jin B B, Qin Y Q and Lu Y Q 2012 *Opt. Mater. Express* **2** 1314
- [44] Lin X W, Wu J B, Hu W, Zheng Z G, Wu Z J, Zhu G, Xu F, Jin B B and Lu Y Q 2011 *AIP Adv.* **1** 032133
- [45] Turnbul G, Robertson D, Smith G, Allen L and Padgett M 1996 *Opt. Commun.* **127** 183
- [46] Hernandez-Serrano A I, Castro-Camus E and Lopez-Mago D 2017 *J. Infrared Millim. Te.* **38** 938
- [47] Furlan W D, Ferrando V, Monsorru J A, Zagrajek P, Czerwińska E and Szustakowski M 2016 *Opt. Lett.* **41** 1748
- [48] Zhu L, Wei X, Wang J, Zhang Z, Li Z, Zhang H, Li S, Wang K, Liu J 2014 *Optical Fiber Communications Conference and Exhibition (OFC)*, March 09–13, 2014, San Francisco, CA, M3K. 7
- [49] Liu C, Liu J, Niu L, Wei X, Wang K and Yang Z 2017 *Sci. Rep.* **7** 3891
- [50] Fallah S, Rouhi K and Abdolali A 2020 *J. Phys. D: Appl. Phys.* **53** 085102
- [51] Rouhi K, Rajabalipanah H and Abdolali A 2019 *Carbon* **149** 125
- [52] Momeni A, Rouhi K, Rajabalipanah H and Abdolali A 2018 *Sci. Rep.* **8** 6200
- [53] Rouhi K, Rajabalipanah H and Abdolali A 2017 *Ann. Phys.* **530** 1700310
- [54] Asgari S and Rahmzadeh M 2020 *Opt. Commun.* **456** 124623
- [55] Liu Z and Bai B 2017 *Opt. Express* **25** 8584
- [56] Qu K, Jia Q and Fisch N J 2017 *Phys. Rev. E* **96** 053207
- [57] Yang Y, Ye X, Niu L, Wang K, Yang Z and Liu J 2020 *Opt. Express* **28** 1417
- [58] Lin J, Yuan X C, Tao S H and Burge R E 2005 *Opt. Lett.* **30** 3266
- [59] Wei X, Liu C, Niu L, Zhang Z, Wang K, Yang Z and Liu J 2015 *Appl. Opt.* **54** 10641
- [60] Wu Z, Wang X, Sun W, Feng S, Han P, Ye J, Yu Y and Zhang Y 2018 *Opt. Express* **26** 1506
- [61] Beijersbergen M W, Coerwinkel R P C, Kristensen M, Woerdman J P 1994 *Opt. Commun.* **112** 321
- [62] Marrucci L, Manzo C and Paparo D 2006 *Phys. Rev. Lett.* **96** 163905
- [63] Marrucci L, Manzo C and Paparo D 2006 *Appl. Phys. Lett.* **88** 221102
- [64] Minasyan A, Trovato C, Degert J, E Freysz, Brasselet E and Abraham E 2017 *Opt. Lett.* **42** 41
- [65] Ge S, Chen P, Shen Z, Sun W, Wang X, Hu W, Zhang Y and Lu Y 2017 *Opt. Express* **25** 12349
- [66] Piccirillo B, D'Ambrosio V, Slussarenko S, Marrucci L and Santamato E 2010 *Appl. Phys. Lett.* **97** 241104
- [67] Rubano A, Cardano F, Piccirillo B and Marrucci L 2019 *J. Opt. Soc. Am. B* **36** D70
- [68] Imai R, Kanda N, Higuchi T, Konishi K and Kuwata-Gonokami M 2014 *Opt. Lett.* **39** 3714
- [69] Wang X, Wang S, Xie Z, Sun W, Feng S, Cui Y, Ye J and Zhang Y 2014 *Opt. Express* **22** 24622
- [70] Imai R, Kanda N, Higuchi T, Zheng Z, Konishi K and Gonokami M K 2012 *Opt. Express* **20** 21896
- [71] Knyazev B A, Choporova Y Y, Mitkov M S, Pavelyev V S, Volodkin B O 2015 *Phys. Rev. Lett.* **115** 163901
- [72] Volodkin B, Choporova Y, Knyazev B, Kulipanov G, Pavelyev V, Soifer V, Vinokurov N 2016 *Opt. Quant. Electron.* **48** 223
- [73] Zhang Y, Liu W, Gao J and Yang X 2018 *Adv. Opt. Mater.* **6** 1701228
- [74] Heckenberg R N, McDuff R, Smith C P and White A G 1992 *Opt. Lett.* **17** 221
- [75] Yao A M and Padgett M J 2011 *Adv. Opt. Photonics* **3** 161
- [76] Zhan Q 2009 *Adv. Opt. Photonics* **1** 1
- [77] Dorn R, Quabis S and Leuchs G 2003 *Phys. Rev. Lett.* **91** 233901
- [78] Khonina S N, Alferov S V and Karpeev S V 2013 *Opt. Lett.* **38** 3223

- [79] He J, Wang X, Hu D, Ye J, Feng S, Kan Q and Zhang Y 2013 *Opt. Express* **21** 20230
- [80] Zhuldybina M, Trudeau C, Ropagnol X, Bolduc M, Zednik R J and Blanchard F 2018 *Photonics North (PN) Conference* June 5–7, 2018, Montreal, Canada
- [81] Taira Y, Nakata Y, Miyamaru F and Takeda M W 2016 *Progress in Electromagnetic Research Symposium (PIERS)*, August 8–11, 2016, Shanghai, China, p. 2396
- [82] Chen Y, Suzuki S and Asada M 2018 *43rd International Conference on Infrared, Millimeter, and Terahertz Waves (IRMMW-THz)*, September 9–14, 2018, Nagoya, Japan
- [83] Zhou H, Dong J, Yan S, Zhou Y and Zhang X 2014 *IEEE Photonics J.* **6** 5900107
- [84] Li X N, Zhou L and Zhao G Z 2019 *Acta Phys. Sin.* **68** 238101 (in Chinese)
- [85] Zang X, Zhu Y, Mao C, Xu W, Ding H, Xie J, Cheng Q, Chen L, Peng Y, Hu Q, Gu M and Zhuang S 2019 *Adv. Opt. Mater.* **7** 1801328
- [86] Kang M, Chen J, Gu B, Li Y, Vuong L T and Wang H T 2012 *Phys. Rev. A* **85** 035801
- [87] Sakamoto M, Oka K, Morita R and Murakami N 2013 *Opt. Lett.* **38** 3661
- [88] Tokizane Y, Oka K and Morita R 2009 *Opt. Express* **17** 14517
- [89] Zhang X D, Su Y H, Ni J C, Wang Z Y, Wang Y L, Wang C W, Ren F F, Zhang Z, Fan H, Zhang W J, Li G Q, Hu Y L, Li J W, Wu D and Chu J R 2017 *Appl. Phys. Lett.* **111** 061901
- [90] Ge S J, Shen Z X, Chen P, Liang X, Wang X K, Hu W, Zhang Y and Lu Y Q 2017 *Crystals* **7** 314
- [91] Li Y, Kim J and Escuti M J 2012 *Appl. Opt.* **51** 8236
- [92] Wu H, Hu W, Hu H C, Lin X W, Zhu G, Choi J W, Chigrinov V and Lu Y Q 2012 *Opt. Express* **20** 16684
- [93] Ala-Laurinaho J, Hirvonen T, Piironen P, Lehto A, Tuovinen J, Räsänen A V and Frisk U 2001 *IEEE T. Antenn. Propag.* **49** 1264
- [94] Salo J, Meltaus J, Noponen E, Salomaa M M, Lönnqvist A, Koskinen T, Viikari V, Säily J, Häkli J, Ala-Laurinaho J, Mallat J and Räsänen A V 2002 *J. Opt. A: Pure Appl. Opt.* **4** S161
- [95] Säily J, Ala-Laurinaho J, Häkli J, Tuovinen J, Lehto A and Räsänen A V 2000 *Electron. Lett.* **36** 111
- [96] Meltaus J, Salo J, Noponen E, Salomaa M M, Viikari V, Lönnqvist A, Koskinen T, Säily J, Häkli J, Ala-Laurinaho J, Mallat J and Räsänen A V 2002 *IEEE MTT-S International Microwave Symposium Digest* 1305
- [97] Xie Z, Wang X, Ye J, Feng S, Akalin T and Zhang Y 2013 *Sci. Rep.* **3** 3347
- [98] Meltaus J, Salo J, Noponen E, Salomaa M M, Viikari V, Lönnqvist A, Koskinen T, Säily J, Häkli J, Ala-Laurinaho J, Mallat J and Räsänen A V 2003 *IEEE T. Microw. Theory* **51** 1274
- [99] Arlt J and Dholakia K 2000 *Opt. Commun.* **177** 297
- [100] Petit R 1980 *Electromagnetic Theory of Gratings* (Berlin: Springer)
- [101] Yu Y Z and Dou W B 2008 *Int. J. Infrared Milli. Waves* **29** 693
- [102] Ferguson B and Zhang X C 2002 *Nat. Materials* **1** 26
- [103] Dhaybi A A, Degert J, Brasselet E, Abraham E and Freysz E 2019 *J. Opt. Soc. Am. B* **36** 12
- [104] Chen Q, Tani M, Jiang Z and Zhang X C 2001 *J. Opt. Soc. Am. B* **18** 823
- [105] Lin Q, Zheng S, Song Q, Zeng X, Cai Y, Li Y, Chen Z, Zha L, Pan X and Xu S 2019 *Opt. Lett.* **44** 887
- [106] Danielson J R, Jameson A D, Tomaino J L, Hui H, Wetzell J D, Lee Y S and Vodopyanov K L 2008 *J. Appl. Phys.* **104** 033111
- [107] Sobhani H and Dadar E 2019 *J. Opt. Soc. Am. A* **36** 1187
- [108] Kreß M, Löffler T, Thomson M D, Dörner R, Gimpel H, Zrost K, Ergler T, Moshhammer R, Morgner U, Ullrich J and Roskos H G 2006 *Nat. Phys.* **2** 327
- [109] Kim K Y, Glowacki J H, Taylor A J and Rodriguez G 2007 *Opt. Express* **15** 4577
- [110] Thomson M D, Kreß M, Löffler T and Roskos H G 2007 *Laser Photonics Rev.* **1** 349
- [111] Bai Y, Song L, Xu R, Li C, Liu P, Zeng Z, Zhang Z, Lu H, Li R and Xu Z 2012 *Phys. Rev. Lett.* **108** 255004
- [112] Wang H, Bai Y, Wu E, Wang Z, Liu P and Liu C 2018 *Phys. Rev. A* **98** 013857
- [113] Wang H, Song Q, Zheng S, Lin Q, Wu E, Ai Y, Liu C and Xu S 2019 *J. Opt.* **21** 095501
- [114] Ivanov M, Thiele I, Bergé L, Skupin S, Buožius D and Vaičiaitis V 2019 *Opt. Lett.* **44** 3889
- [115] E Y, Jin Q, Tcypkin A and Zhang X C 2019 *Appl. Phys. Lett.* **113** 181103
- [116] Jin Q, E Y, Williams K, Dai J and Zhang X C 2017 *Appl. Phys. Lett.* **111** 071103
- [117] Dey I, Jana K, Fedorov V Y, Koulouklidis A D, Mondal A, Shaikh M, Sarkar D, Lad A D, Tzortzakos S, Couairon A and Kumar G R 2017 *Nat. Commun.* **8** 1184
- [118] Jin Q, E Y, Zhang L, Zhang C, Tcypkin A, Kozlov S and Zhang X C 2018 *43rd International Conference on Infrared, Millimeter, and Terahertz Waves (IRMMW-THz)*, September 9–14, Nagoya, Japan
- [119] Jiang G, Zhang L, Zhang S and Zhang C 2018 *Infrared, Millimeter-Wave, and Terahertz Technologies V, Proc. SPIE*, November 9, 2018, 10826 108261G
- [120] Piesiewicz R, Jacob M, Koch M, Schoebel J and Kürner T 2008 *IEEE J. Sel. Top. Quant.* **14** 421
- [121] Federici J and Moeller L 2010 *J. Appl. Phys.* **107** 111101
- [122] Han C, Bicen A O and Akyildiz I F 2016 *IEEE T. Signal Proces* **64** 910
- [123] Wei X, Zhu L, Zhang Z, Wang K, Liu J and Wang J 2014 *Conference on Lasers and Electro-Optics (CLEO)—Laser Science to Photonic Application*, June 8–13, 2014, San Jose CA, STu2F2.
- [124] Fickler R, Lapkiewicz R, Plick W N, Krenn M, Schaeff C, Ramelow S and Zeilinger A 2012 *Science* **338** 640
- [125] Nagatsuma T, Ducournau G and Renaud C C 2016 *Nat. Photon.* **10** 371
- [126] Hirata A, Kosugi T, Takahashi H, Yamaguchi R, Nakajima F, Furuta T, Ito H, Sugahara H, Sato Y and Nagatsuma T 2006 *IEEE T. Microw. Theory* **54** 1937
- [127] Takahashi H, Hirata A, Takeuchi J, Kukutsu N, Kosugi T and Murata K 2012 *15th European Microwave Week-Space for Microwaves Conference Proceedings*, p. 313
- [128] Cherry S 2004 *IEEE Spectrum* **41** 58
- [129] Bozinovic N, Yue Y, Ren Y, Tur M, Kristensen P, Huang H, Willner A E and Ramachandran S 2013 *Science* **340** 1545
- [130] Wang J, Yang J Y, Fazal I M, Ahmed N, Yan Y, Huang H, Ren Y, Yue Y, Dolinar S, Tur M and Willner A E 2012 *Nat. Photon.* **6** 488
- [131] Wang Z, Zhang N and Yuan X C 2011 *Opt. Express* **19** 482
- [132] Gao X, Huang S, Zhou J, Wei Y, Gao C, Zhang X and Gu W 2013 *J. Opt.* **15** 105401
- [133] Bespalov V G 2016 *Russ. Phys. J.* **58** 1420
- [134] Jepsen P U, Cooke D G and Koch M 2011 *Laser Photonics Rev.* **5** 124
- [135] Jansen C, Wietzke S, Peters O, Scheller M, Vieweg N, Salhi M, Krumbholz N, Jördens C, Hochrein T and Koch M 2010 *Appl. Opt.* **49** E48
- [136] Cocker T L, Huber M A, Eisele M, Plankl M, Mooshammer F, Sandner F, Peller D, Repp J and Huber R 2016 *Progress in Electromagnetic Research Symposium (PIERS)*, August 8–11, Shanghai, China, p. 3339
- [137] Long Z, Wang T, You C, Yang Z, Wang K and Liu J 2019 *Appl. Opt.* **58** 2731
- [138] Liu K, Cheng Y, Yang Z, Wang H, Qin Y and Li X 2015 *IEEE Antenn. Wirel. Pr.* **14** 711
- [139] Chen S C, Du L H, Meng K, Li J, Zhai Z H, Shi Q W, Li Z R and Zhu L G 2019 *Opt. Lett.* **44** 21
- [140] Guo Y, Ling F, Li H, Zhou S, Ji J and Yao J 2019 *Appl. Opt.* **58** 6244
- [141] Bretschneider S, Eggeling C and Hell S W 2007 *Phys. Rev. Lett.* **98** 218130
- [142] Baek I H, Ahn K J, Kang B J, Bae S, Hong B H, Yeom D I, Lee K, Jeong Y U and Rotermund F 2013 *Appl. Phys. Lett.* **102** 191109
- [143] Hebling J, Yeh K, Hoffmann M C and Nelson K A 2008 *IEEE J. Sel. Top. Quant.* **14** 345
- [144] Sharma G, Al-Naib I, Hafez H, Morandotti R, Cooke D G, Ozaki T 2012 *Opt. Express* **20** 18016
- [145] Cao J C and Lei J C 2003 *Phys. Rev. B* **67** 085309
- [146] Wen H, Wiczler M and Lindenberg A M 2008 *Phys. Rev. B* **78** 125203
- [147] Sanvitto D, Marchetti F M, Szymańska M H, Tosi G, Baudisch M, Laussy F P, Krizhanovskii D N, Skolnick M S, Marrucci L, Lemaître A, Bloch J, Tejedor C and Viña L 2010 *Nat. Phys.* **6** 527
- [148] Toyoda K, Miyamoto K, Aoki N, Morita R and Omatsu T 2012 *Nano Lett.* **12** 3645
- [149] Toyoda K, Takahashi F, Takizawa S, Tokizane Y, Miyamoto K, Morita R and Omatsu T 2013 *Phys. Rev. Lett.* **110** 143603
- [150] Takahashi F, Miyamoto K, Hidai H, Yamane K, Morita R and Omatsu T 2016 *Sci. Rep.* **6** 21738
- [151] Nanni E A, Huang W R, Hong K H, Ravi K, Fallahi A, Moriena G, Miller R J D and Kärtner F X 2015 *Nat. Commun.* **6** 8486

- [152] Anzolin G, Tamburini F, Bianchini A, Umbriaco G and Barbieri C 2008 *Astro. Astrophys.* **488** 1159
- [153] Tamburini F, Anzolin G, Bianchini A and Barbieri C 2006 *Phys. Rev. Lett.* **97** 163903
- [154] Barbieri C, Naletto G and Occhipinti T, *et al.* 2009 *J. Mod. Optic.* **56** 261
- [155] Serabyn E, Mawet D and Burruss R 2010 *Nature* **464** 1018
- [156] Lee J H, Foo G, Johnson E G and Swartzlander Jr G A 2006 *Phys. Rev. Lett.* **97** 053901
- [157] Bekshaev A, Bliokh K Y and Soskin M 2011 *J. Opt.* **13** 053001
- [158] Dehnen H 1973 *Int. J. Theor. Phys.* **7** 467
- [159] Carini P, Feng L L, Li M and Ruffini R 1992 *Phys. Rev. D* **46** 5407
- [160] Feng L L and Lee W L 2001 *Int. J. Mod. Phys. D* **10** 961
- [161] Broderick A E, Fish V L, Doeleman S S and Loeb A 2009 *Astrophys. J.* **697** 45
- [162] Jenkins C 2008 *Mon. Not. R. Astron. Soc.* **384** 515
- [163] Delacroix C, Absil O, Forsberg P, Mawet D, Christiaens V, Karlsson M, Boccaletti A, Baudoz P, Kuitinen M, Vartiainen I, Surdej J and Habraken S 2013 *Astron. Astrophys.* **553** A98